International Journal of Solids and Structures 49 (2012) 2460–2470

Contents lists available at SciVerse ScienceDirect

International Journal of Solids and Structures

journal homepage: www.elsevier.com/locate/ijsolstr

Interlaminar stresses and energy release rates in delaminated orthotropic composite plates

András Szekrényes *

Budapest University of Technology and Economics, Department of Applied Mechanics, Müegyetem rkp. 5, 1111 Budapest, Building MM, Hungary

ARTICLE INFO

Article history:
Received 6 February 2012
Received in revised form 23 April 2012
Available online 30 May 2012

Keywords:
Delamination
Energy release rate
Laminated plate
Mixed mode II/III fracture
J-integral

ABSTRACT

The classical laminated plate theory is applied to calculate the stresses and energy release rate function in symmetrically delaminated orthotropic plates. First, the equilibrium of classical plate forces, moments and interfacial shear stresses is formulated. Second, the displacement continuity between the interface plane of a double-plate model was considered. The governing equation system of the double-plate model consists of ten equations. As an example a delaminated, orthotropic, simply-supported plate subjected to a point force is analyzed. The distribution of the plate forces as well as the interlaminar shear stresses over the uncracked part were determined. Moreover, the mode-II and mode-III energy release rate distributions along the crack front were calculated by the *J*-integral. The 3D finite element model of the delaminated composite plate was also created. The results indicate a reasonably good agreement between analysis and numerical calculation.

1. Introduction

Laminated composite plates have many industrial applications, e.g., the fields of bridge and bodywork construction, aeroplanes and finally but not least ship construction can be mentioned. Delamination is one of the major damage mode in laminated fiber-reinforced polymer matrix composite materials (Brunner and Flüeler, 2005; Brunner et al., 2008), on which the paper is focusing. Mechanically, the formation of cracks and delamination surfaces can be characterized by means of the energy-based principles of fracture mechanics (Anderson, 2005), however it must be mentioned that for many structural applications (e.g., aircrafts) strength-stiffness criteria are still used for design (Tsai, 1992). The energy release rate (ERR) is the basic parameter dimensioning the structures against crack initiation and propagation. The limit value of the ERR is called the critical ERR (CERR), which can be determined using standard (or nonstandard) test methods. It has to be noted that some standards specify a minimum bending stiffness requirements for the material (e.g., ISO 15024 for mode-I). Beam tests, in general involve simple geometry and reduction schemes. Although for the mode-I (Wilkins et al., 1982; ISO15024, 2001), mode-II (Russel and Street, 1982; JIS7086, 1993) and mixed-mode I/II fracture (Reeder and Crews, 1990; ASTMD6671-01, 2001) there is a consensus to use simple beam tests, for mode-III (Lee, 1993; Li and O'Brien, 1996; Farshad and Flüeler, 1998; de Moura et al., 2009; Szekrényes, 2009a; de Morais and Pereira, 2009; Browning et al., 2010, 2011; de Morais et al., 2011; Pereira et al., 2011) there is not yet an internationally accepted test. Also, the combination of the mode-I and mode-II fractures have the greatest attention in the society of researchers and engineers (e.g., Plain and Tong, 2011; da Silva et al., 2011; Jumel et al., 2011). On the contrary, mixed-mode I/III (Pereira and de Morais, 2009; Szekrényes, 2009b), II/III (Szekrényes, 2007; de Morais and Pereira, 2008; Suemasu et al., 2010; Kondo et al., 2011) and I/II/III (Marat-Mendes and Freitas, 2010; Davidson and Sediles, 2011; Szekrényes, 2011) were investigated only in the 21st century. The mode-III fracture involves significant difficulties: first pure mode-III condition is impossible to be achieved, second the geometry of the test samples is also a critical point. Beam specimens are in general very stiff, plate specimens are much more difficult to be manufactured.

An important issue in mixed-mode fracture is the separation of fracture modes. For beams (mixed-mode I/II) the energy-based method developed by Williams (1988) must be mentioned first. This so-called global method is valid only for symmetrically delaminated beams, moreover the top and bottom subbeams must have identical mechanical properties. A local method was developed by Suo and Hutchinson (1990). The ERR was calculated based on beam theory, but the mode ratio was calculated by solving the problem of a semi infinite crack by the distributed dislocation method (Hills et al., 1996). The main aspect is that it works for unsymmetrically delaminated beams too. A similar model was also proposed by Davidson et al. (1995). Mode separation in cracked bodies is also possible by using the *J*-integral (Rice, 1968;

* Tel.: +36 1 463 1170; fax: +36 1 463 3471.
E-mail address: szeki@mm.bme.hu

0020-7683/$ - see front matter © 2012 Elsevier Ltd. All rights reserved.
http://dx.doi.org/10.1016/j.ijsolstr.2012.05.010

Cherepanov, 1997) by utilizing field theories, either for plane or 3D problems (Shivakumar and Raju, 1992; Rigby and Aliabadi, 1998). The virtual crack-closure technique (VCCT) is a powerful numerical method for the calculation of ERR and mode ratio. (e.g., Marat-Mendes and Freitas, 2010). Apart from that there is a plate theory based method in conjunction with finite element analysis, see e.g., (Sankar and Sonik, 1995; Davidson et al., 2000). The so-called crack tip force method (CTFM) (Park and Sankar, 2002) is based on similar considerations as the VCCT. The main problem of the FE models is that for plates the 3D model should be constructed with relatively high mesh resolution and in most of the FE packages the VCCT is not available as a built-in command. Considering the mode separation problem the development of new approaches is still in progress (see e.g. Wang and Harvey, 2012; Valvo, 2012).

In this paper the classical laminated plate theory (CLPT) is complemented with a flexible joint. The governing equations of mixed-mode II/III delamination problems are formulated for a double plate model. The equilibrium of in-plane forces, interfacial shear stresses, bending and twisting moments is considered. Apart from that the displacement continuity between the top and bottom plates is derived. The boundary value problem is solved for a simply-supported orthotropic plate with midplane delamination. The whole problem is solved in two steps. First CLPT is applied, second the flexible joint model is utilized. The resultant stress field and energy release rate are calculated by superimposing the results of the two subproblems.

2. Classical laminate plate model with flexible joint

Fig. 1 shows two differentially small plate elements taken from the top (a) and bottom (b) layers of an uncracked orthotropic plate. Here we consider only balanced laminated plates, i.e., the top and bottom layers are also orthotropic and their lay-up is symmetric with respect to the local mid-planes. It is assumed that the deflection of the top and bottom plate elements are the same and are equal to $w(x,y)$. The equilibrium of the in-plane plate forces and the interfacial shear stresses leads to (see Fig. 1):

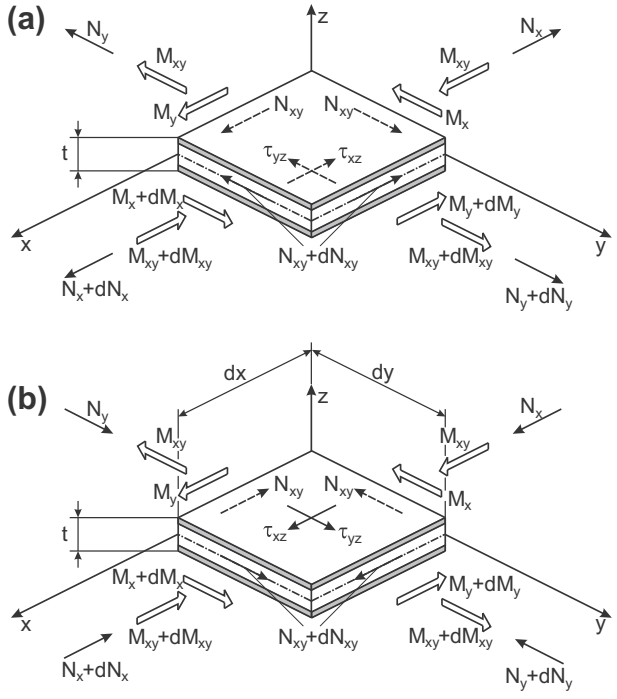

Fig. 1. Equilibrium of the top (a) and bottom (b) differential plate elements.

$$\frac{\partial N_x}{\partial x}-\frac{\partial N_{xy}}{\partial y}=\tau_{xz},\quad -\frac{\partial N_{xy}}{\partial x}+\frac{\partial N_y}{\partial y}=\tau_{yz} \tag{1}$$

where N_x, N_y are the in-plane normal forces, N_{xy} is the in-plane shear force, $\tau_{xz}=\tau_{xz}(x,y)$ and $\tau_{yz}=\tau_{yz}(x,y)$ are the interfacial shear stresses, respectively. Considering the moment equilibrium about axes x and y we obtain:

$$\frac{\partial M_x}{\partial x}+\frac{\partial M_{xy}}{\partial y}=-\tau_{xz}\frac{t}{2},\frac{\partial M_{xy}}{\partial x}+\frac{\partial M_y}{\partial y}=-\tau_{yz}\frac{t}{2} \tag{2}$$

where M_x, M_y and M_{xy} are the bending and twisting moments. The direct and inverse relations between forces and strains are (Reddy, 2004):

$$\begin{bmatrix}N_x\\N_y\\N_{xy}\end{bmatrix}=\begin{bmatrix}A_{11}&A_{12}&0\\A_{12}&A_{22}&0\\0&0&A_{66}\end{bmatrix}\begin{bmatrix}\varepsilon_x^0\\\varepsilon_y^0\\\gamma_{xy}^0\end{bmatrix} \tag{3}$$

$$\begin{bmatrix}\varepsilon_x^0\\\varepsilon_y^0\\\gamma_{xy}^0\end{bmatrix}=\begin{bmatrix}a_{11}&a_{12}&0\\a_{12}&a_{22}&0\\0&0&a_{66}\end{bmatrix}\begin{bmatrix}N_x\\N_y\\N_{xy}\end{bmatrix} \tag{4}$$

where A_{ij} are the corresponding extensional stiffnesses, while a_{ij} are the compliances calculated from the inverse of the extensional stiffness matrix (Reddy, 2004; Kollár and Springer, 2003). Following the basic equations of CLPT the moment–curvature relationships are (Kollár and Springer, 2003):

$$\begin{bmatrix}M_x\\M_y\\M_{xy}\end{bmatrix}=\begin{bmatrix}D_{11}&D_{12}&0\\D_{12}&D_{22}&0\\0&0&D_{66}\end{bmatrix}\begin{bmatrix}-w_{,xx}\\-w_{,yy}\\-2w_{,xy}\end{bmatrix} \tag{5}$$

where D_{ij} is the corresponding bending/twisting stiffness. As a next step we formulate the continuity conditions over the interface of the uncracked portion of a delaminated plate system. Along the crack front a flexible joint model (Wang and Qiao, 2004) is applied. Fig. 2. presents the possible sources of the in-plane displacements: in-plane forces (a), bending (b) and finally the interface shear deformation (c and d). The resultant displacement from these effects along the interface of the top plate is:

$$u|_{z=-t/2}=\int(a_{11}N_x+a_{12}N_y)dx-\frac{t}{2}\frac{\partial w}{\partial x}-k_{sh}^{55}\tau_{xz}=0 \tag{6}$$

$$v|_{z=-t/2}=\int(a_{12}N_x+a_{22}N_y)dy-\frac{t}{2}\frac{\partial w}{\partial y}-k_{sh}^{44}\tau_{yz}=0 \tag{7}$$

where:

$$k_{sh}^{55}=\sum_{k=1}^{N_l}\frac{z_{k+1}-z_k}{3\overline{C}_{55}^{(k)}},\quad k_{sh}^{44}=\sum_{k=1}^{N_l}\frac{z_{k+1}-z_k}{3\overline{C}_{44}^{(k)}} \tag{8}$$

are the shear compliances and are calculated as the generalization of the one given by Suhir (1986). Moreover $\overline{C}_{55}$ and $\overline{C}_{44}$ are the shear stiffnesses for a single laminate (Reddy, 2004). A third condition must be satisfied for plates: the shear strain must be equal to zero along the interface. In this respect three effects should be considered based on Fig. 3 (Chou and Pagano, 1967): in-plane shear force (a), twisting moment (b) and the shear strain induced by interface shear stresses (c), i.e.,

$$\gamma_{xy}\Big|_{z=-t/2}=-a_{66}N_{xy}-t\frac{\partial^2 w}{\partial x\partial y}-\left(k_{sh}^{55}\frac{\partial\tau_{xz}}{\partial y}+k_{sh}^{44}\frac{\partial\tau_{yz}}{\partial x}\right)=0 \tag{9}$$

Eqs. (6), (7) and (9) can be obtained also by formulating the continuity conditions for the bottom plate element. In order to obtain a kinematically compatible displacement field Eqs. (6) and (7) must satisfy the following equation (Chou and Pagano, 1967):

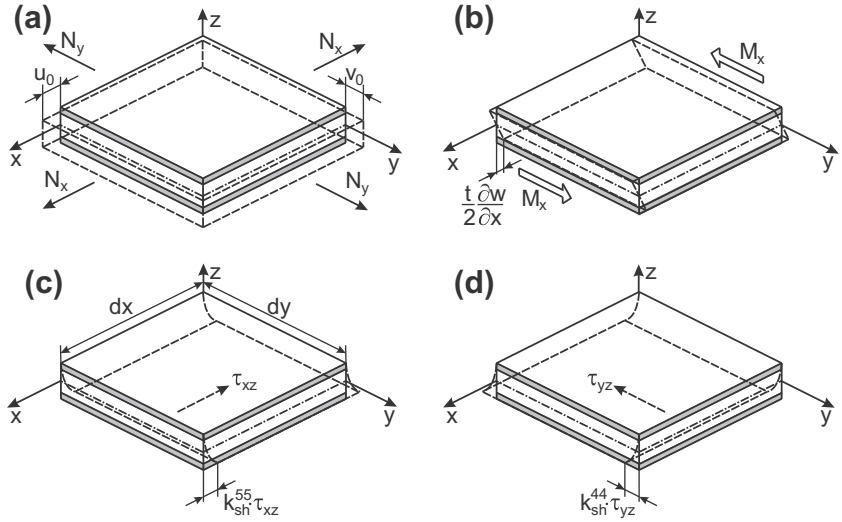

Fig. 2. Deformations of the top plate element under in-plane forces (a), bending (b) and interface shear stresses (c,d).

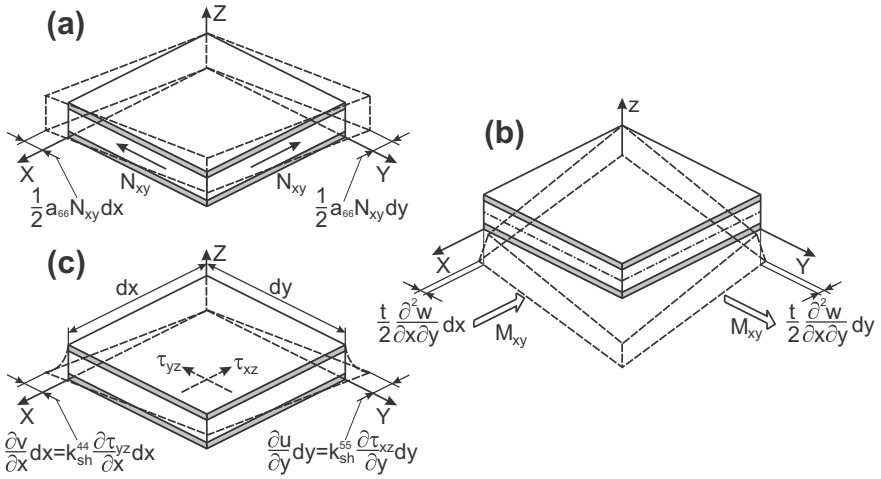

Fig. 3. Deformations of the top plate element under in-plane shear force (a), torsion (b) and interface shear stresses (c).

$$\gamma_{xy}\Big|_{z=-t/2} = \frac{\partial u}{\partial y} + \frac{\partial v}{\partial x}\Big|_{z=-t/2} \tag{10}$$

The second and third terms in Eqs. (6) and (7) satisfy automatically this condition. On the contrary, with respect to the first terms in the same equations the following relationship can be obtained:

$$\frac{\partial^2 N_{xy}}{\partial x \partial y} = -\frac{1}{a_{66}}\left(a_{11}\frac{\partial^2 N_x}{\partial y^2} + a_{22}\frac{\partial^2 N_y}{\partial x^2} + a_{12}\left\{\frac{\partial^2 N_x}{\partial x^2} + \frac{\partial^2 N_y}{\partial y^2}\right\}\right) \tag{11}$$

The basic equations for the uncracked portion of laminated plates with a flexible joint are given by Eqs. (1) and (2) (equilibrium equations), (5) (moment–curvature relationships), (6), (7) and (9) (kinematic conditions), which are totally ten equations building a system of partial differential equations (PDE). The ten parameters are: N_x, N_y, N_{xy}, $M_x, M_y, M_{xy}, \tau_{xz}, \tau_{yz}, \partial w/\partial x$ and $\partial w/\partial y$. Utilizing the moment–curvature equations (Eqs. (5)) and taking them back into Eq. (2), it is possible to obtain the governing differential equation of the plate deflection for the uncracked region in the form of:

$$D_{11}\frac{\partial^4 w}{\partial x^4} + 2(D_{12} + 2D_{66})\frac{\partial^4 w}{\partial x^2 \partial y^2} + D_{22}\frac{\partial^4 w}{\partial y^4} = \frac{t}{2}\left(\frac{\partial \tau_{xz}}{\partial x} + \frac{\partial \tau_{yz}}{\partial y}\right) \tag{12}$$

i.e., the inhomogeneity is caused by the interfacial shear stresses.

3. Governing equations of in-plane forces

In this section we derive the PDEs for the in-plane forces. The first step is that we express $\partial w/\partial x, \partial w/\partial y$ and $\partial^2 w/\partial x \partial y$ from Eqs. (6), (7) and (9), respectively. Then we take them back into (Eq. (5)). Afterwards $\tau_{xz}(x,y)$ and $\tau_{yz}(x,y)$ are calculated from Eq. (1), the derivative of $N_{xy}(x,y)$ is given by Eq. (11), all of them should be taken back into the expressions of moments. Finally, the first derivatives of the moments are put into the equilibrium equations (Eq. (2)). This procedure leads to the following equations:

$$A_1\frac{\partial^4 N_x}{\partial x^4} + A_2\frac{\partial^2 N_x}{\partial x^2 \partial y^2} + A_3\frac{\partial^2 N_x}{\partial x^2} + A_4\frac{\partial^4 N_x}{\partial y^4} + A_5\frac{\partial^2 N_x}{\partial y^2} + A_6\frac{\partial^4 N_y}{\partial x^4} + A_7\frac{\partial^2 N_y}{\partial x^2 \partial y^2} + A_8\frac{\partial^2 N_y}{\partial x^2} + A_9\frac{\partial^4 N_y}{\partial y^4} + A_{10}\frac{\partial^2 N_y}{\partial y^2} = 0 \tag{13}$$

$$B_1\frac{\partial^4 N_y}{\partial x^4} + B_2\frac{\partial^2 N_y}{\partial x^2 \partial y^2} + B_3\frac{\partial^2 N_y}{\partial x^2} + B_4\frac{\partial^4 N_y}{\partial y^4} + B_5\frac{\partial^2 N_y}{\partial y^2} + B_6\frac{\partial^4 N_x}{\partial x^4} + B_7\frac{\partial^2 N_x}{\partial x^2 \partial y^2} + B_8\frac{\partial^2 N_x}{\partial x^2} + B_9\frac{\partial^4 N_x}{\partial y^4} + B_{10}\frac{\partial^2 N_x}{\partial y^2} = 0 \tag{14}$$

where the coefficients are collected in Appendix A. In the next section we present the solution for a simply-supported thin orthotropic plate subjected to a point force.

4. Solution of a simply-supported delaminated plate

Let us consider now Fig. 4, where the whole problem is treated as the sum of two subproblems. Problem (a) in Fig. 4a is a delaminated composite plate treated as a general plate bending problem using CLPT. Problem (b) implies that the plate is loaded by the interfacial shear tractions, $\tau_{xz}(x,y)$ and $\tau_{yz}(x,y)$. This problem is solved by using the equations presented in Sections 2,3 providing an improvement with respect to the original (a) problem.

4.1. Problem (a) – simply-supported stepped thickness plate

This problem is treated as a stepped thickness plate (Guo, 1997), where the different bending stiffness of the delaminated and uncracked parts are considered (see Fig. 4). The deflection of the cracked (1) and uncracked (2) plate portions are:

$$\begin{aligned} &w_1^a(x,y): 0 \leqslant x \leqslant a, \quad 0 \leqslant y \leqslant b \\ &w_2^a(x,y): -c \leqslant x \leqslant 0, \quad 0 \leqslant y \leqslant b \end{aligned} \tag{15}$$

In accordance with Lévy plate formulation (Reddy, 2004), we have:

$$w_1^a(x,y) = \sum_{n=1}^{\infty} W_{1n}^a(x)\sin\beta y, \quad w_2^a(x,y) = \sum_{n=1}^{\infty} W_{2n}^a(x)\sin\beta y \tag{16}$$

where $\beta = \frac{n\pi}{b}$. Taking the deflections back into the general governing equation of laminated plates (Reddy, 2004) we obtain:

$$D_{11}^{(1)}\frac{d^4W_{1n}^a(x)}{dx^4} - 2\beta^2(D_{12}^{(1)} + 2D_{66}^{(1)})\frac{d^2W_{1n}^a(x)}{dx^2} + \beta^4 D_{22}^{(1)} W_{1n}^a(x) = Q_n \tag{17}$$

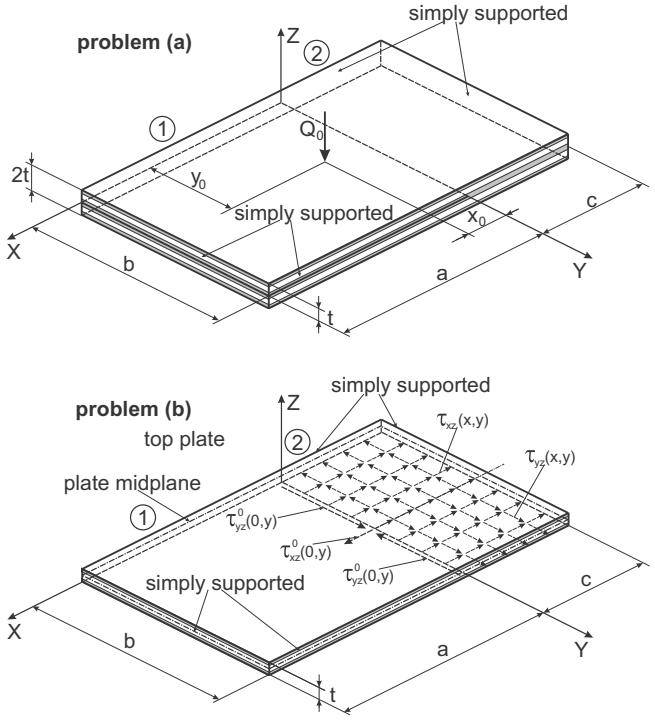

Fig. 4. A simply-supported delaminated plate subjected to point force. Subproblem (a): stepped thickness plate. Subproblem (b): top plate subject to shear tractions.

where:

$$Q_n = \frac{2Q_0}{b}\delta(x - x_0)\sin\beta y_0 \tag{18}$$

In the undelaminated part the deflection is governed by:

$$D_{11}^{(2)}\frac{d^4W_{2n}^a(x)}{dx^4} - 2\beta^2\left(D_{12}^{(2)} + 2D_{66}^{(2)}\right)\frac{d^2W_{2n}^a(x)}{dx^2} + \beta^4 D_{22}^{(2)} W_{2n}^a(x) = 0 \tag{19}$$

The solution functions are:

$$W_{1n}^a(x) = \sum_{i=1}^{4} A_{in} e^{\lambda_i^{(1)}x} + W_{1np}^a(x), \quad \text{if } x_0 \leqslant x \leqslant a \tag{20}$$

where the particular solution is:

$$W_{1np}^a(x) = \frac{Q_0\sin\beta y_0}{2\beta^2 b D_1^*}\left(\frac{e^{\lambda_1^{(1)}(x-x_0)}}{\lambda_1^{(1)}} - \frac{e^{\lambda_2^{(1)}(x-x_0)}}{\lambda_2^{(1)}} + \frac{e^{\lambda_3^{(1)}(x-x_0)}}{\lambda_3^{(1)}} - \frac{e^{\lambda_4^{(1)}(x-x_0)}}{\lambda_4^{(1)}}\right) \tag{21}$$

Moreover:

$$\begin{aligned} W_{1n}^a(x) &= \sum_{i=1}^{4} A_{in} e^{\lambda_i^{(1)}x}, \quad \text{if } 0 \leqslant x \leqslant x_0 \\ W_{2n}^a(x) &= \sum_{i=1}^{4} B_{in} e^{\lambda_i^{(2)}x}, \quad \text{if } -c \leqslant x \leqslant 0 \end{aligned} \tag{22}$$

where A_{in} and B_{in} are constants and the subscript, n refers to the actual Fourier term. The characteristic roots based on Eqs. (17), (19) are:

$$\begin{aligned} \lambda_1^{(k)} &= \sqrt{\left((D_{12}^{(k)} + 2D_{66}^{(k)})^2 - D_k^*\right)/D_{11}^{(k)}}\beta, \quad \lambda_3^{(k)} = -\lambda_1^{(k)}, \quad k = 1,2 \\ \lambda_2^{(k)} &= \sqrt{\left((D_{12}^{(k)} + 2D_{66}^{(k)})^2 + D_k^*\right)/D_{11}^{(k)}}\beta, \quad \lambda_4^{(k)} = -\lambda_2^{(k)}, \quad k = 1,2 \end{aligned} \tag{23}$$

where k refers to the delaminated (1) and uncracked (2) part, and: $D_k^* = \sqrt{(D_{12}^{(k)} + 2D_{66}^{(k)})^2 - D_{11}^{(k)}D_{22}^{(k)}}$. To determine the constants the following boundary conditions (B.C.s) must be satisfied:

$$W_{1n}^a(a) = 0, \quad D_{11}^{(1)}\frac{d^2W_{1n}^a}{dx^2} - \beta^2 D_{12}^{(1)} W_{1n}^a\Big|_{x=a} = 0 \tag{24}$$

$$W_{2n}^a(-c) = 0, \quad D_{11}^{(2)}\frac{d^2W_{2n}^a}{dx^2} - \beta^2 D_{12}^{(2)} W_{2n}^a\Big|_{x=-c} \tag{25}$$

Moreover, the continuity of the deflection, slope, bending moment and effective (Kirchhoff) shear force involves four more conditions (Guo, 1997):

$$W_{1n}^a(0) = W_{2n}^a(0), \quad \left.\frac{dW_{1n}^a}{dx}\right|_{x=0} = \left.\frac{dW_{2n}^a}{dx}\right|_{x=0} \tag{26}$$

$$-D_{11}^{(1)}\frac{d^2W_{1n}^a}{dx^2} + \beta^2 D_{12}^{(1)} W_{1n}^a\Big|_{x=0} = -D_{11}^{(2)}\frac{d^2W_{2n}^a}{dx^2} + \beta^2 D_{12}^{(2)} W_{2n}^a\Big|_{x=0} \tag{27}$$

$$\begin{aligned} &D_{11}^{(1)}\frac{d^3W_{1n}^a}{dx^3} - \beta^2\left(D_{12}^{(1)} + 4D_{66}^{(1)}\right)\frac{dW_{1n}^a}{dx}\Big|_{x=0} \\ &= D_{11}^{(2)}\frac{d^3W_{2n}^a}{dx^3} - \beta^2\left(D_{12}^{(2)} + 4D_{66}^{(2)}\right)\frac{dW_{2n}^a}{dx}\Big|_{x=0} \end{aligned} \tag{28}$$

If the deflection is known, the interlaminar shear stresses can be obtained for each layer using the 3D equilibrium equations (Reddy, 2004, p. 250).

4.2. Problem (b) – simply-supported plate subject to shear tractions

Since the plate is symmetric, it is sufficient to analyze only the top plates of the cracked and uncracked regions. Consequently, the bending and extensional stiffnesses for problem (b) are equal to the halves of those in problem (a). Similar to the deflection we shall approximate the in-plane forces and shear stress by Fourier series in the y direction as:

$$N_x = \sum_{n=1}^{\infty} n_{xn}(x)\sin\beta y, \quad N_y = \sum_{n=1}^{\infty} n_{yn}(x)\sin\beta y,$$
$$N_{xy} = \sum_{n=1}^{\infty} n_{xyn}(x)\cos\beta y \tag{29}$$

From Eq. (20) it is clear that $W_n(x)$ has a homogeneous and a particular solutions as well. It is a reasonable assumption, that the shear stresses, τ_{xz} and τ_{yz} have only particular solutions. Moreover the in-plane forces are:

$$n_{xn} = n^h_{xn} + n^p_{xn}, \quad n_{yn} = n^h_{yn} + n^p_{yn}, \quad n_{xyn} = n^h_{xyn} + n^p_{xyn} \tag{30}$$

i.e., even the forces have homogeneous and particular solutions. Eqs. (6) and (7) are satisfied only by the particular solutions of the forces, thus from Eqs. (13) and (14) we have:

$$A_1\frac{d^4 n^p_{xn}}{dx^4} + A_{23}\frac{d^2 n^p_{xn}}{dx^2} + A_{45}n^h_{xn} + A_6\frac{d^4 n^p_{yn}}{dx^4} + A_{78}\frac{d^2 n^p_{yn}}{dx^2} + A_{910}n^p_{yn} = 0$$
$$B_1\frac{d^4 n^p_{yn}}{dx^4} + B_{23}\frac{d^2 n^p_{yn}}{dx^2} + B_{45}n^p_{yn} + B_6\frac{d^4 n^p_{xn}}{dx^4} + B_{78}\frac{d^2 n^p_{xn}}{dx^2} + B_{910}n^p_{xn} = 0 \tag{31}$$

where the constants are: $A_{23} = -A_2\beta^2 + A_3$, $A_{45} = A_4\beta^4 - A_5\beta^2$, $A_{78} = -A_7\beta^2 + A_8$, $A_{910} = A_9\beta^4 - A_{10}\beta^2$, $B_{23} = -B_2\beta^2 + B_3$, $B_{45} = B_4\beta^4 - B_5\beta^2$, $B_{78} = -B_7\beta^2 + B_8$, $B_{910} = B_9\beta^4 - B_{10}\beta^2$. We assume the following solutions:

$$n^p_{xn}(x) = \sum_{i=1}^{8} N_{in}e^{\lambda_i x}, \quad n^p_{yn}(x) = \sum_{i=1}^{8} M_{in}e^{\lambda_i x} \tag{32}$$

Utilizing these solutions, from Eq. (31) we obtain:

$$\begin{bmatrix} Q_{11} & Q_{12} \\ Q_{21} & Q_{22} \end{bmatrix}^{(i)} \begin{bmatrix} N_{in} \\ M_{in} \end{bmatrix} = \begin{bmatrix} 0 \\ 0 \end{bmatrix} \tag{33}$$

The characteristic equation is obtained by setting the determinant of the matrix in Eq. (33) to zero, i.e., $Q_{11}Q_{22} - Q_{12}Q_{21} = 0$. It is important to note that the constants in Eq. (32) are not independent of each other, e.g., $M_{in} = -[Q_{11}/Q_{12}]^{(i)}N_{in}$. The next step is the calculation of N_{xy} from Eq. (11):

$$n^p_{xyn}(x) = -\frac{1}{a_{66}}\left\{\beta\int(a_{11}n^p_{xn} + a_{12}n^p_{yn})dx - \frac{1}{\beta}(a_{12}n^p_{xn,x} + a_{12}n^p_{yn,x})\right\} \tag{34}$$

Based on Eqs. (29) and (1) the shear stresses are approximated as:

$$\tau_{xz}(x,y) = \sum_{n=1}^{\infty} T_n(x)\sin\beta y, \quad \tau_{yz}(x,y) = \sum_{n=1}^{\infty} R_n(x)\cos\beta y \tag{35}$$

where T_n and R_n can be determined by using Eq. (1):

$$T_n(x) = \sum_{i=1}^{8} C_{in}e^{\lambda_i x}, \quad R_n(x) = \sum_{i=1}^{8} D_{in}e^{\lambda_i x} \tag{36}$$

where the constants C_{in} and D_{in} depend on N_{in} and M_{in}:

$$C_{in} = -\left(N_{in}(a^{(2)}_{11b}\beta^2 - (a^{(2)}_{12b} + a^{(2)}_{66b})\lambda_i^2) - M_{in}(a^{(2)}_{22b}\lambda_i^2 - a^{(2)}_{12b}\beta^2)\right)/(a^{(2)}_{66b}\lambda_i)$$
$$D_{in} = \left(N_{in}(a^{(2)}_{11b}\beta^2 - a^{(2)}_{12b}\lambda_i^2) - M_{in}(a^{(2)}_{22b}\lambda^2 - (a^{(2)}_{12b} + a^{(2)}_{66b})\beta^2)\right)/(a^{(2)}_{66b}\beta) \tag{37}$$

In Eqs. (32) and (36) there are eight characteristic roots, however it can be proven that only two of them result in kinematically compatible displacement fields. In general, it is $\pm$ the smallest real root. Therefore six of the eight constants in Eq. (36) are zero: $C_{in} = D_{in} = 0,\ i = 3\ldots8$. The deflections in problem (b) are approximated as:

$$w^b_1(x,y) = \sum_{n=1}^{\infty} W^b_{1n}(x)\sin\beta y, \quad w^b_2(x,y) = \sum_{n=1}^{\infty} W^b_{2n}(x)\sin\beta y \tag{38}$$

The deflection of the delaminated part is governed by Eqs. (19), while in the uncracked part it is governed by Eq. (12). The solutions are obtained in the usual way:

$$W^b_{1n}(x) = \sum_{i=1}^{4} G_{in}e^{\lambda^{(1)}_i x}, \quad W^b_{2n}(x) = \sum_{i=1}^{4} H_{in}e^{\lambda^{(2)}_i x} + W^b_{2np}(x) \tag{39}$$

where the particular solution of the latter is obtained by taking back Eq. (35) into Eq. (12):

$$W^b_{2np}(x) = \frac{1}{2}\sum_{i=1}^{8}\frac{D^{(2)}_{11b}t(C_i\lambda_i - D_i\beta)e^{\lambda_i x}}{\left[\lambda_i^2 D^{(2)}_{11b} - \beta^2(D^{(2)}_{12b} + 2D^{(2)}_{66b})\right]^2 - \beta^4 D^{*2}_{2b}} \tag{40}$$

where: $D^*_{2b} = \sqrt{(D^{(2)}_{12b})^2 + 4D^{(2)}_{12b}D^{(2)}_{66b} + 4(D^{(2)}_{66b})^2 - D^{(2)}_{11b}D^{(2)}_{22b}}$. Apparently, it is necessary to calculate the homogeneous solutions of the in-plane forces. Eqs. (6) and (7) can be satisfied only solutions having the same characteristic roots as the homogeneous solution of the deflection in the uncracked part. Therefore, we assume the following solutions:

$$n^h_{nx}(x) = \sum_{i=1}^{4} X_{in}e^{\lambda^{(2)}_i x}, \quad n^h_{ny}(x) = \sum_{i=1}^{4} Y_{in}e^{\lambda^{(2)}_i x}, \quad n^h_{nxy}(x) = \sum_{i=1}^{4} K_{in}e^{\lambda^{(2)}_i x} \tag{41}$$

where the constants can be obtained by Eqs. (6), (7) and (9) in the form of:

$$X_{in} = H_{in}\frac{t}{2}\frac{a^{(2)}_{12b}\beta^2 + a^{(2)}_{22b}\lambda_i^{(2)^2}}{a^{(2)}_{11b}a^{(2)}_{22b} - (a^{(2)}_{12b})^2},$$
$$Y_{in} = -H_{in}\frac{t}{2}\frac{a^{(2)}_{11b}\beta^2 + a^{(2)}_{12b}\lambda_i^{(2)^2}}{a^{(2)}_{11b}a^{(2)}_{22b} - (a^{(2)}_{12b})^2} \tag{42}$$

$$K_{in} = -H_{in}t\frac{\beta\lambda^{(2)}_i}{a^{(2)}_{66b}} \tag{43}$$

thus, the constants X_{in}, Y_{in} and K_{in} depend equally on H_{in} (see Eq. (39)). Finally, we need to formulate the B.C.s. In Eqs. (39) and (36) we have ten unknown constants. Eight of them can be determined through W^b_{2n} and W^b_{1n}. Essentially, these are the same as Eqs. (24)–(28). Two more conditions can be formulated with respect to the shear stresses. The shear stress, τ_{xz} must vanish at the end of the uncracked portion, therefore we have:

$$T_n(-c) = 0 \tag{44}$$

The last condition is obtained based on the axial equilibrium of the resultant forces coming from the shear tractions along the midplanes of the cracked and uncracked portions (refer to Fig. 4) (Wang and Qiao, 2004). However, in this respect we need to use two conditions. First, we assume that in the y direction the distribution of τ_{xz} in problem (b) is the same as that in problem (a). For that we utilize the following:

$$\tau^{(a)}_{xz2}\Big|_{z=0} = \sum_{n=1}^{\infty} T^0_n(x)\sin\beta y \tag{45}$$

where $\tau^{(a)}_{xz2} = \tau^{(a)}_{xz2}(x,y,z)$ is the shear stress at the layer containing the midplane of the uncracked part determined from the 3D equilibrium equations for problem (a). Finally, the tenth condition is:

$$T_n(0) = CT_n^0(x) \tag{46}$$

where C is determined by:

$$\int_0^b \int_{x_0}^a \tau_{xz1}^{(a)}\Big|_{z=0} dxdy + \int_0^b \int_0^{x_0} \tau_{xz1}^{(a)}\Big|_{z=0} dxdy - \int_0^b \int_{-c}^0 \tau_{xz} dxdy = 0 \tag{47}$$

where $\tau_{xz1}^{(a)}$ is the shear stress in the layer containing the $z = 0$ plane in the delaminated region from problem (a), while τ_{xz} is the shear stress in problem (b). In the following section we discuss the details how the ERR is calculated.

5. Energy release rate and mode mixity

In the general 3D case the J-integral is (Shivakumar and Raju, 1992):

$$J_k = \int_C (Wn_k - \sigma_{ij}u_{i,k}n_j)ds + \int_A (W\delta_{k3} - \sigma_{i3}u_{i,k})_{,3}dA, \quad k = 1,2$$
$$J_3 = \int_C (W_3 n_1 - \sigma_{3j}u_{3,1}n_j)ds \tag{48}$$

where W and W_3 are the strain energy densities defined as:

$$W = \int_0^{\varepsilon_{ij}} \sigma_{ij}d\varepsilon_{ij}, W_3 = \int_0^{\varepsilon_{3j}} \sigma_{3j}d\varepsilon_{3j} \tag{49}$$

and n_k is the outward normal vector of the contour C, δ_{ij} is the Kronecker tensor, σ_{ij} is the stress tensor ($\sigma_{ij}n_j$ is the traction vector), u_i is the displacement vector, A is the area enclosed by contour C. The mode separation of the J-integral is possible by a direct method (Rigby and Aliabadi, 1998):

$$J_1 = J_I + J_{II} + J_{III}, \quad J_2 = -2\sqrt{J_I J_{II}}, \quad J_3 = J_{III} \tag{50}$$

In our case $x_1 = x$, $x_2 = z$ and $x_3 = y$. For the calculation we apply a zero-area path, in other words the integration bounds are x=−0 and x=+0 around the crack tip. This way the surface integral in Eq. (48) becomes zero.

5.1. J-integral for problem (a)

For problem (a) the strain energy densities become:

$$W = \frac{1}{2}(\sigma_x\varepsilon_x + \sigma_y\varepsilon_y + \tau_{xy}\gamma_{xy}), \quad W_3 = \frac{1}{2}(\sigma_y\varepsilon_y + \tau_{xy}\gamma_{xy}) \tag{51}$$

where the stresses can be determined layerwise (Reddy, 2004, p. 100), moreover $\varepsilon_x = -w_{,xx}\cdot z$, $\varepsilon_y = -w_{,yy}\cdot z$, $\gamma_{xy} = -2w_{,xy}\cdot z$. However, the terms related to σ_y and ϵ_y in J_1 and J_3 should be ignored. This can be justified by the incompatible displacement field illustrated in Fig. 5. It is seen that the CLPT model predicts erroneously the displacement field and so the stress state in the transition zone, which can be counteracted only by ignoring the terms in question. Thus, the J-integrals are:

$$J_{1a} = -\frac{1}{2}\left(M_{x1}^a w_{1,xx}^a\Big|_{x=+0} - M_{x2}^a w_{2,xx}^a\Big|_{x=-0}\right) + 2\left(M_{xy1}^a w_{1,xy}^a\Big|_{x=+0} - M_{xy2}^a w_{2,xy}^a\Big|_{x=-0}\right) \tag{52}$$

$$J_{2a} = 0, J_{3a} = 2\left(M_{xy1}^a w_{1,xy}^a\Big|_{x=+0} - M_{xy2}^a w_{2,xy}^a\Big|_{x=-0}\right) \tag{53}$$

where in the moments (1) refers to the delaminated, (2) refers to the uncracked portion of the plate (see Fig. 4). It is important to note

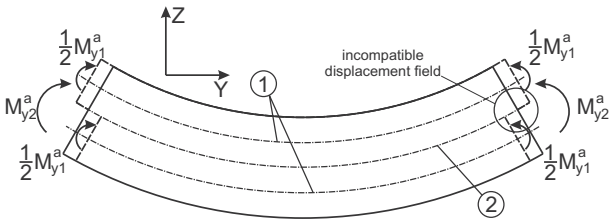

Fig. 5. Incompatible displacement field predicted by classical laminated plate theory.

the subscripts 1 and 2 on the right hand side refer to the actual component of the J-integral. Based on Eq. (50) we have:

$$J_{IIa}(y) = -\frac{1}{2}\left(M_{x1}^a w_{1,xx}^a\Big|_{x=+0} - M_{x2}^a w_{2,xx}^a\Big|_{x=-0}\right) \tag{54}$$

$$J_{IIIa}(y) = 2\left(M_{xy1}^a w_{1,xy}^a\Big|_{x=+0} - M_{xy2}^a w_{2,xy}^a\Big|_{x=-0}\right) \tag{55}$$

5.2. J-integral for problem (b)

For problem (b) the strain energy densities for the delaminated (1) part are the same as those given by Eq. (51), for the uncracked (2) part they are:

$$W^{(2)} = \frac{1}{2}\left(\sigma_x^{(2)}\varepsilon_x^{(2)} + \sigma_y^{(2)}\varepsilon_y^{(2)} + \tau_{xy}^{(2)}\gamma_{xy}^{(2)} + \tau_{xz}^{(2)}\gamma_{xz}^{(2)} + \tau_{yz}^{(2)}\gamma_{yz}^{(2)}\right)$$
$$W_3^{(2)} = \frac{1}{2}\left(\sigma_y^{(2)}\varepsilon_y^{(2)} + \tau_{xy}^{(2)}\gamma_{xy}^{(2)} + \tau_{yz}^{(2)}\gamma_{yz}^{(2)}\right) \tag{56}$$

In the uncracked part due to the presence of the in-plane normal and shear forces in Eq. (56) we have: $\varepsilon_x = \varepsilon_x^0 - w_{,xx}\cdot z$, $\varepsilon_y = \varepsilon_y^0 - w_{,yy}\cdot z$, $\gamma_{xy} = \gamma_{xy}^0 - 2w_{,xy}\cdot z$, where ϵ_x^0, ϵ_y^0 and γ_{xy}^0, can be calculated by Eq. (4). Again, the terms related to σ_y and ϵ_y in J_{1b} and J_{3b} should be ignored. Calculating the mode-II and mode-III integrals we have: J_{IIb}=2 $\cdot J_{1b} - 2\cdot J_{3b}$ and J_{IIb}=2 $\cdot J_{3b}$ where a multiplication by 2 is necessary because we have two plates (top and bottom), and for problem (b) only one of them have been analyzed. Thus, we obtain:

$$J_{IIb} = 2\left\{-\frac{1}{2}\left(M_{x1}^b w_{1,xx}^b\Big|_{x=+0} - M_{x2}^b w_{2,xx}^b\Big|_{x=-0}\right) + \frac{1}{2}N_x\varepsilon_x^0|_{x=-0} + \sum_{k=1}^{N_l}\int_{z_k}^{z_{k+1}} \tau_{xz}^{(k)}(w_{2,x}^b - \frac{1}{2}u_{2,z}^{b(k)})dz|_{x=-0}\right\} \tag{57}$$

$$J_{IIIb} = 2\left\{2\left(M_{xy1}^b w_{1,xy}^b\Big|_{x=+0} - M_{xy2}^b w_{2,xy}^b\Big|_{x=-0}\right) + N_{xy}\left(\frac{1}{2}\gamma_{xy}^0 + v_{2,x}^{0b}\right)|_{x=-0} - \frac{1}{2}\sum_{k=1}^{N_l}\int_{z_k}^{z_{k+1}} \tau_{yz}^{(k)}v_{2,z}^{b(k)}dz|_{x=-0}\right\} \tag{58}$$

where based on Eqs. (6) and (7):

$$u_{2,z}^{b(k)} = k_{sh}^{55}\frac{\partial\tau_{xz}^{(2)(k)}}{\partial z}, \quad v_{2,z}^{b(k)} = k_{sh}^{44}\frac{\partial\tau_{yz}^{(2)(k)}}{\partial z},$$
$$v_2^{0b} = \int (a_{12b}^{(2)}N_x + a_{22b}^{(2)}N_y)dy \tag{59}$$

where the first two are the derivatives of the in-plane displacements induced by the shear stresses in the k^{th} layer. Finally, the ERRs are: $G_{II} = J_{IIa} + J_{IIb}$, $G_{III} = J_{IIIa} + J_{IIIb}$. The mode mixity ($G_{II}/G_{III}$) can also be calculated at each y location along the crack front.

6. Results and discussion

The properties of the analyzed simply-supported plate were (refer to Fig. 4): $a = 105$ mm (crack length), $c = 45$ mm (uncracked length), $b = 100$ mm (plate width), $t = 2$ mm (half plate thickness), $Q_0 = 1000$ N (point force magnitude), $x_0 = 31$ mm, $y_0 = 50$ mm (point of action coordinates of Q_0). The plate is made of a carbon/epoxy material, the lay-up of the plate was $[\pm 45_2^{\circ f}; 0^\circ_{12}; \pm 45_2^{\circ f}]$ for the delaminated and $[\pm 45_2^{\circ f}; 0^\circ_{12}; \pm 45_2^{\circ f}]_s$ for the uncracked part. The properties of the individual laminae are given by Table 1 (Kollár and Springer, 2003). The computation was performed in the code MAPLE. First, problem (a) in Fig. 4 was solved varying the number of Fourier series terms (N) by creating a for-do cycle. Then, from the 3D equilibrium equations (Reddy, 2004) the transverse shear stress distributions were calculated. The next step was the solution of problem (b) in Fig. 5, the system of equations was constructed using Eqs. (36) and (39) by utilizing the B.C.s given by Eqs. (24)–(28). It was assumed that the interfacial shear stresses have the same distributions in terms of z as those of problem (a). The shear stress (τ_{xz}) for problem (b) was determined from Eq. (47). Afterwards, the in-plane normal and shear forces were determined from Eqs. (32), (34) and (41), while the ERRs were calculated using the J-integral. The convergence of the results was analyzed and it was found that after the 13th Fourier term there was no change in the displacement field, stresses, forces and ERRs.

6.1. Finite element model

The 3D finite element model of the plate was created in the code ANSYS 12 using 8 node layered solid elements. 50, 78 and 10 elements were applied along the plate width (y), length (x) and thickness (z), respectively. The global element size was 2 mm × 2 mm × 0.4 mm. In the vicinity of the crack tip a refined mesh was constructed including trapezoid shape elements. The z displacements of the contact nodes over the delaminated surface were imposed to be the same. The mode-II and mode-III ERRs were calculated by the VCCT, the size of the crack tip elements were $\Delta x = 0.2$ mm, $\Delta y = 0.2$ mm and $\Delta z = 2$ mm. For the determination of G_{II} and G_{III} along the delamination front a so-called MACRO was written in the ANSYS Design and Parametric Language.

6.2. Classical plate theory results

Figs. 6 and 7 demonstrate the distribution of the in-plane normal and shear forces over the interface of the undelaminated region of the top plate ($N = 19$). In the case of N_x both solutions are symmetric in the y direction, in contrast, the shear force N_{xy} has asymmetric distributions. It is important to note that the homogeneous part of N_{xy} is induced by the twisting curvature of the top and bottom plate elements (refer to Fig. 3b), while the particular solution is related to the interfacial shear stresses. The interface shear stresses are plotted in Fig. 8. Similar to the particular solution of in-plane forces, they decay to zero behind the crack front. In Fig. 9 the normal stress distributions are shown at two points along the crack front. It is shown that both σ_x and σ_y decrease by approximately 10% compared to problem (a). This is not a miscalculation, the deflection of the uncracked part is different in problem (a) than in problem (b).

Fig. 10 shows the distribution of the shear stresses, τ_{xz} and τ_{yz} over the thickness at $x = 0$. It is seen that τ_{xz} changes significantly – by 42% – compared to problem (a). Also, τ_{yz} is improved by more than twice of its original value (increase by 165%). Thus, the shear deformation of the crack front results in significant changes in the interlaminar shear stress distributions. It must be mentioned that the stresses from N_x, N_y and N_{xy} are negligibly small, therefore these were not considered.

6.3. Classical plate theory against VCCT

The mode-II, mode-III ERRs and the mode ratio along the crack front are shown by Fig. 11. The symbols show the result of the VCCT, while the curves represent the plate theory solutions. The solution of problem (a) provides the major part of the ERRs, but problem (b) provides a reasonable improvement for the mode-II

Table 1
Elastic properties of single carbon/epoxy composite laminates.

	E_x [GPa]	E_y [GPa]	E_z [GPa]	G_{yz} [GPa]	G_{xz} [GPa]	G_{xy} [GPa]	ν_{yz} [–]	ν_{xz} [–]	ν_{xz} [–]
$\pm 45^{\circ f}$	16.39	16.39	16.4	5.46	16.4	5.46	0.5	0.3	0.5
0°	148	9.65	9.65	4.91	3.71	4.66	0.27	0.3	0.25

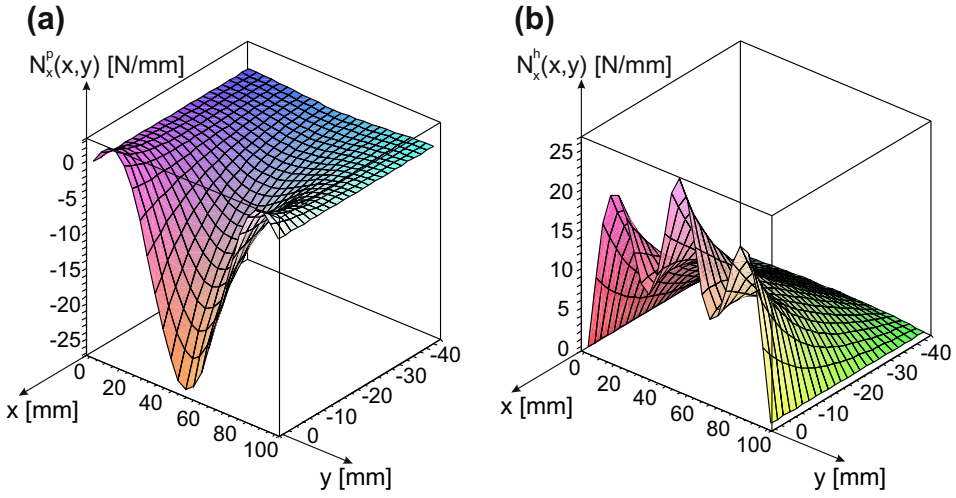

Fig. 6. Distribution of the particular (a) and homogeneous (b) solutions of N_x.

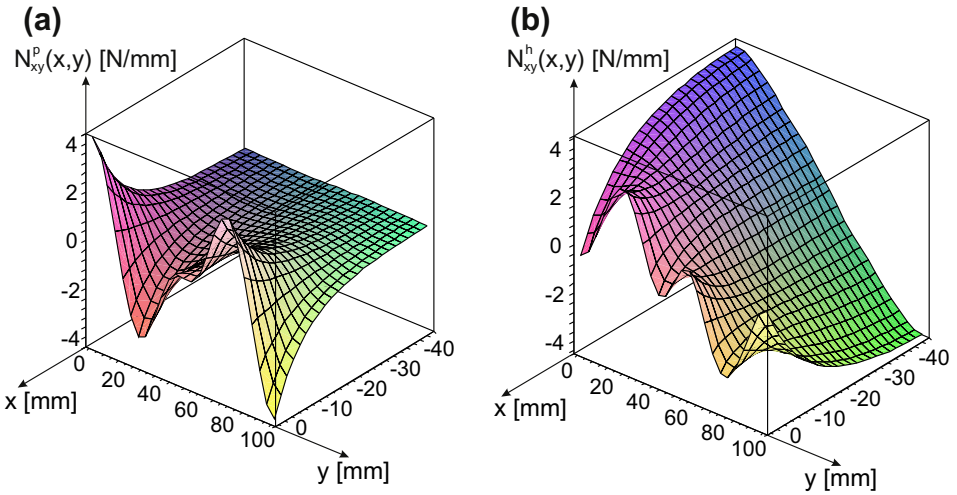

Fig. 7. Distribution of the particular (a) and homogeneous (b) solutions of N_{xy}.

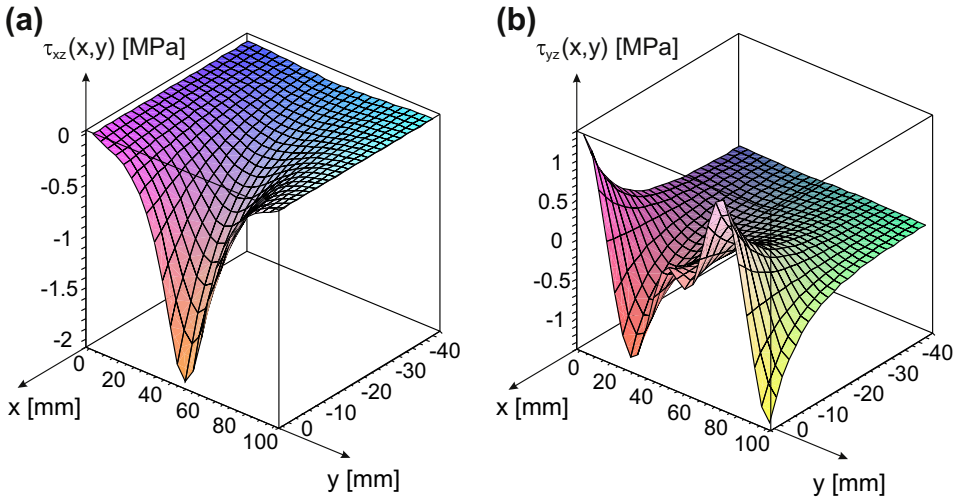

Fig. 8. Distribution of the interface shear stresses: τ_{xz} (a), τ_{yz} (b).

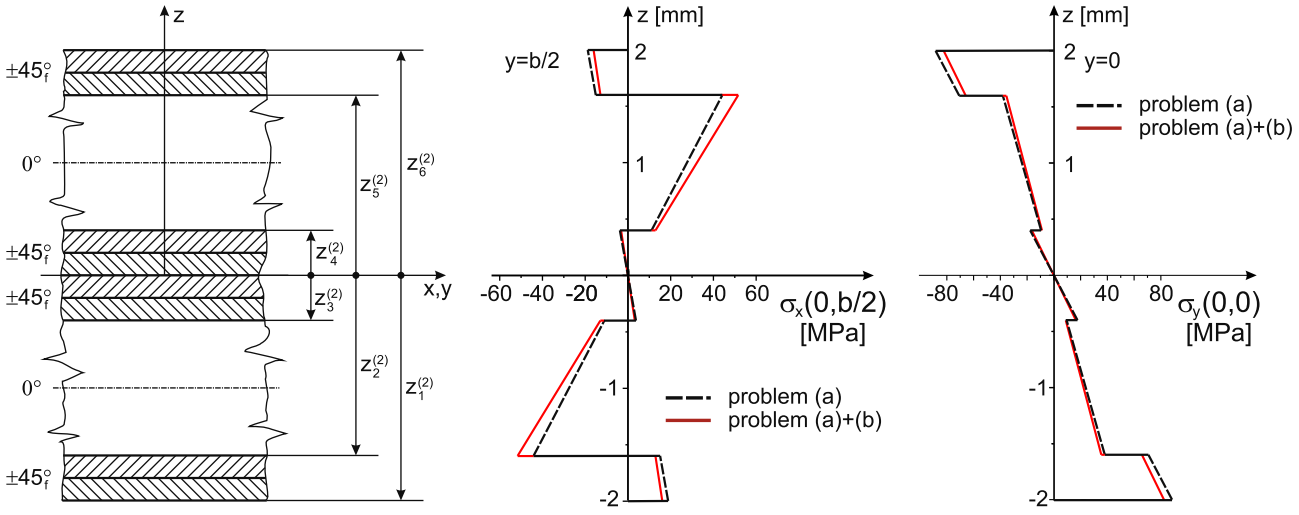

Fig. 9. Distribution of the normal stresses σ_x and σ_y at two points in the crack front.

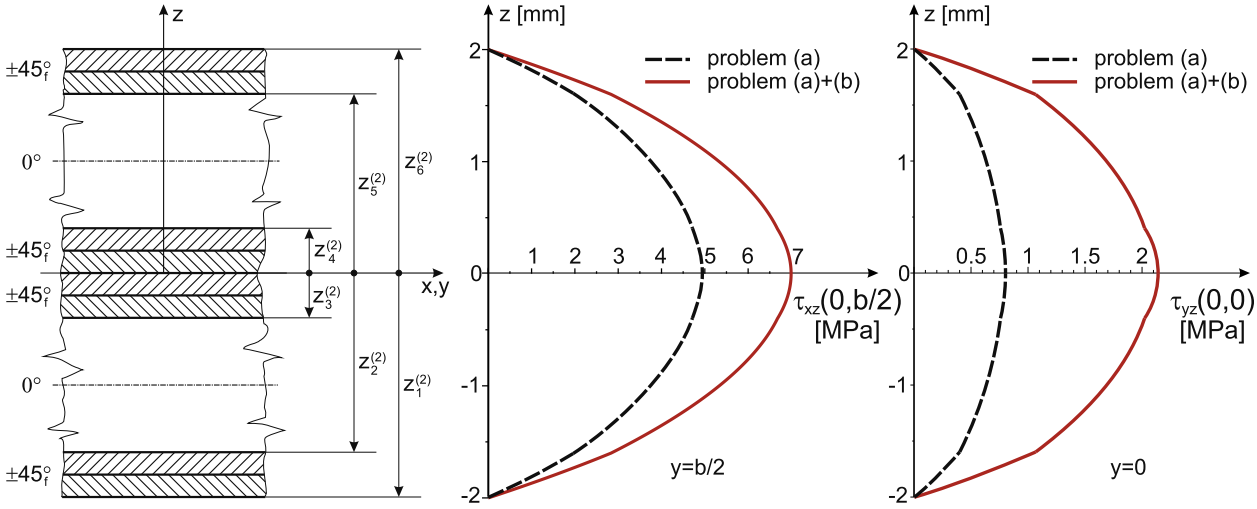

Fig. 10. Distribution of the shear stresses τ_{xz} and τ_{yz} at two points in the crack front.

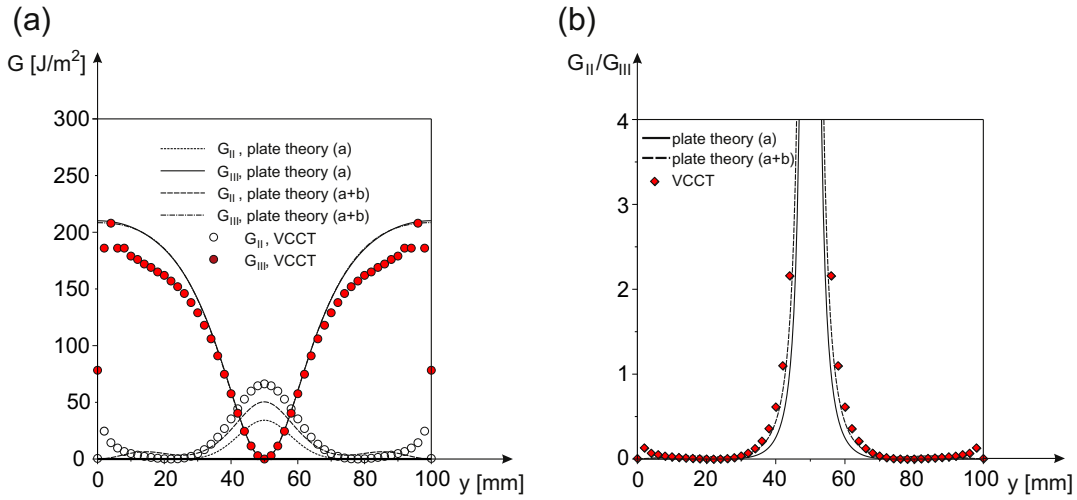

Fig. 11. Energy release rate distributions (a) and mode ratios (b) by laminated plate theory (Lévy solution) and FE analysis.

ERR. It can be seen that the contribution of the mode-III ERR is negligible (Fig. 11a). While the VCCT predicts that the mode-III ERR decays suddenly near the edges, there is not any decay in accordance with the CLPT solution. In other words, edge effects are not captured properly by the CLPT model. The mode ratio (G_{II}/G_{III}) is depicted in Fig. 11b. The plate theory solution slightly underestimates the mode ratio by VCCT, however the nature of the curves matches well with the numerical result. Also, it is clear that the improvement related to the shear deformation of the crack front is reasonable.

Fig. 12 shows the relative error of the CLPT approach compared to the VCCT. The error becomes huge near the edges for both components, but for the mode-II component it is also significant between the edge and the midpart of the crack front.

The overall agreement between the VCCT and plate theory methods is fairly good, the differences can be attributed to the transverse shear and edge effects. It should also be kept in mind that the VCCT method is mesh sensitive to a certain degree and the convergence study of the VCCT was outside the scope of this report.

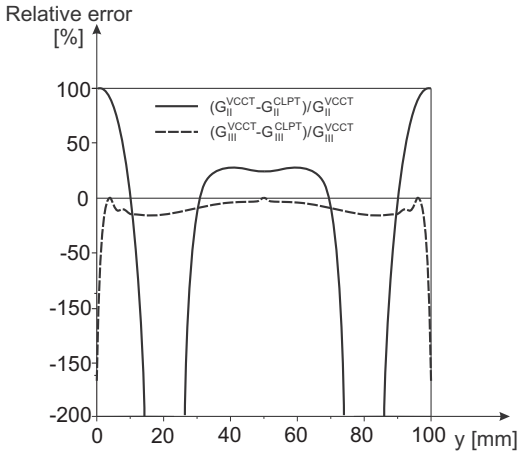

Fig. 12. Relative error of the CLPT solution compared to VCCT results for problem (a) + (b).

7. Summary and conclusions

An analytical plate theory approach utilizing a flexible joint model has been presented to determine the displacement and stress fields in symmetrically delaminated, layered composite plates subject to bending. The energy release rates have been calculated using the 3D *J*-integral. The results have been compared to those of a 3D finite element model and a fairly good agreement has been found. It has been shown that the interface shear stress contributes significantly only to the mode-II energy release rate. Also, the effect of crack front shear deformation on the interlaminar shear stresses was found to be significant.

The possible application field of the presented method is the fracture mechanics of composite materials. In the last few years test methods involving the bending of delaminated composite plates have been developed (Lee, 1993; Li and O'Brien, 1996; Farshad and Flüeler, 1998; de Morais and Pereira, 2009, 2008; Pereira and de Morais, 2009) for mode-III, mixed-mode II/III and I/III. Although the application of the proposed formulation is lengthy, it can help the experimentalists to reduce measured data by plate specimens in an easier way than it is usually provided by VCCT.

Considering the available methods for the calculation of the ERR in plates the first choice is in general the VCCT. However, for a 3D FE model the computation could be lengthy, especially if the model has relatively large dimensions. Moreover in the crack tip a refined mesh should be constructed to obtain accurate ERR values. Finally, in most of the commercial FE packages the VCCT has not yet been implemented. In this respect the present work provides another possibility for plate bending problems including delamination. The disadvantages of the proposed formulation are the facts that the ERRs can be calculated in two steps, the method can be applied for plates with through the width crack and involving simple B.C.s wherein the Lévy plate formulation can be applied. On the other hand the two level computation can be performed in the same MAPLE worksheet and the data of the model (material and geometrical properties, load position and magnitude) can be very simply varied compared to a FE model. The present model can further be developed for the following cases: plates with asymmetric delamination and unbalanced lay-up, moderately thick plates utilizing the Reissner–Mindlin plate theory, thick plates utilizing elasticity solution, which involves a similar mathematical formulation and finally but not least plates with more complex B.C.s, like free edges and point supports.

Acknowledgments

This paper was supported by the János Bolyai Research Scholarship of the Hungarian Academy of Sciences. This work is connected to the scientific program of the "Development of quality-oriented and harmonized R + D + I strategy and functional model at BME" project. This project is supported by the New Hungary Development Plan (Project ID: TÁMOP-4.2.1/B-09/1/KMR-2010-0002).

Appendix A. Coefficients for Eqs. 13,14

$$A_1 = 2\frac{D_{11}k_{sh}^{55}a^* + k_{sh}^{44}a_{12}D^*}{a_{66}t}, \quad A_2 = 2\frac{k_{sh}^{55}(a_{11}D_{11} + a^*D_{66}) + k_{sh}^{44}a_{11}D^*}{a_{66}t} \tag{A.1}$$

$$A_3 = -\frac{2(a_{11}D_{11} + a_{12}D^*)}{t} + \frac{ta^*}{2a_{66}}, \quad A_4 = \frac{2a_{11}D_{66}k_{sh}^{55}}{a_{66}t},$$
$$A_5 = -\frac{2a_{11}D_{66}}{t} + \frac{ta^*}{2a_{66}} \tag{A.2}$$

$$A_3 = -\frac{2(a_{11}D_{11} + a_{12}D^*)}{t} + \frac{ta^*}{2a_{66}}, \quad A_4 = \frac{2a_{11}D_{66}k_{sh}^{55}}{a_{66}t},$$
$$A_5 = -\frac{2a_{11}D_{66}}{t} + \frac{ta^*}{2a_{66}} \tag{A.3}$$

$$A_6 = 2a_{22}\frac{D_{11}k_{sh}^{55} + k_{sh}^{44}D^*}{a_{66}t}, \quad A_7 = 2\frac{k_{sh}^{55}(a_{12}D_{11} + a_{22}D_{66}) + k_{sh}^{44}a^*D^*}{a_{66}t},$$
$$A_9 = A_4\frac{a_{12}}{a_{11}} \tag{A.4}$$

$$A_8 = -\frac{2(a_{12}D_{11} + a_{22}D^*)}{t} + \frac{ta_{22}}{2a_{66}t}, A_{10} = A_5\frac{a_{12}}{a_{11}},$$
$$B_1 = \frac{2a_{22}D_{66}k_{sh}^{44}}{a_{66}t} \tag{A.5}$$

$$B_2 = 2\frac{k_{sh}^{55}a_{22}D^* + k_{sh}^{44}(a_{22}D_{22} + a^*D_{66})}{a_{66}t},$$
$$B_3 = \frac{a_{22}}{a_{11}}A_5, \quad B_4 = 2\frac{D_{22}k_{sh}^{44}a^* + k_{sh}^{55}a_{12}D^*}{a_{66}t} \tag{A.6}$$

$$B_5 = -\frac{2(a_{22}D_{22} + a_{12}D^*)}{t} + \frac{ta^*}{2a_{66}}, \quad B_6 = \frac{a_{12}}{a_{22}}B_1, \quad B_8 = A_{10},$$
$$B_9 = 2a_{11}\frac{D_{22}k_{sh}^{44} + k_{sh}^{55}D^*}{a_{66}t} \tag{A.7}$$

$$B_7 = 2\frac{k_{sh}^{44}(a_{12}D_{22} + a_{11}D_{66}) + k_{sh}^{55}a^*D^*}{a_{66}t},$$
$$B_{10} = -\frac{2(a_{12}D_{22} + a_{11}D^*)}{t} + \frac{ta_{11}}{2a_{66}} \tag{A.8}$$

where $a^* = a_{12} + a_{66}$ and $D^* = D_{12} + D_{66}$.

References

Anderson, T.L., 2005. Fracture Mechanics – Fundamentals and Applications. CRC Press, third edition, Taylor & Francis Group, Boca Raton, London, New York, Singapore.

ASTMD6671-01., 2001. Test method for mixed mode I–II interlaminar fracture toughness of unidirectional fiber reinforced polymer matrix composites. American Society for Testing and Materials, West Conshohocken, PA.

Browning, G., Carlsson, L.A., Ratcliffe, J.G., 2010. Redesign of the ECT test for mode III delamination testing. part I: Finite element analysis. Journal of Composite Materials 44, 1867–1881.

Browning, G., Carlsson, L.A., Ratcliffe, J.G., 2011. Modification of the edge crack torsion specimen for mode III delamination testing. Part II – Experimental study. Journal of Composite Materials 45, 2633–2640.

Brunner, A.J., Blackman, B.R.K., Davies, P., 2008. A status report on delamination resistance testing of polymer-matrix composites. Engineering Fracture Mechanics 75, 2779–2794.

Brunner, A.J., Flüeler, P., 2005. Prospects in fracture mechanics of "'engineering" laminates. Engineering Fracture Mechanics 72, 899–908.

Cherepanov, G.P., 1997. Methods of Fracture Mechanics: Solid Matter Physics. Kluwer Academic Publishers., Dordrecht, Boston, London.

Chou, P.C., Pagano, N.J., 1967. Elasticity – Tensor Dyadic and Engineering Approaches. D. Van Nostrand Company Inc., Princeton, New Jersey, Toronto, London.

Davidson, B.A., Sediles, F.O., 2011. Mixed-mode I–II–III delamination toughness determination via a shear-torsion-bending test. Composites Part A: Applied Science and Manufacturing 42, 589–603.

Davidson, B.D., Hu, H., Schapery, R.A., 1995. An analytical crack-tip element for layered elastic structures. Journal of Applied Mechanics 62, 294–305.

Davidson, B.D., Yu, L., Hu, H., 2000. Determination of energy release rate and mode mix in three-dimensional layered structures using plate theory. International Journal of Fracture 105, 81–104.

Farshad, M., Flüeler, P., 1998. Investigation of mode III fracture toughness using an anti-clastic plate bending method. Engineering Fracture Mechanics 60, 597603.

Guo, S.J., 1997. Vibration analysis of stepped thickness plates. Journal of Sound and Vibration 204, 645–657.

Hills, D.A., Kelly, P.A., Dai, D.N., Korsunsky, A.M., 1996. Solution of Crack Problems, The Distributed Dislocation Technique. Kluwer Academic Publishers, Dordrecht, Boston, London.

ISO15024, 2001. Fibre-reinforced plastic composites – Determination of mode I interlaminar fracture toughness, *GIC*, for unidirectionally reinforced materials. International Organization for Standardization.

JIS7086., 1993. Testing methods for interlaminar fracture toughness of carbon fiber reinforced plastics. Japanese Standards Association, Japanese Industrial Standards. Tokyo, Japan.

Jumel, J., Budzik, M.K., Shanahan, M.E.R., 2011. Process zone in the single cantilever beam under transverse loading. Part I: Theoretical analysis. Theoretical and Applied Fracture Mechanics 56, 7–12.

Kollár, L.P., Springer, G.S., 2003. Mechanics of Composite Structures. Cambridge University Press, Cambridge, New York, Melbourne, Madrid, Cape Town, Singapore, São Paolo.

Kondo, A., Sato, Y., Suemasu, H., Aoki, Y., 2011. Fracture resistance of carbon/epoxy composite laminates under mixed-mode II and III failure and its dependence on fracture morphology. Advanced Composite Materials 20, 405–418.

Lee, S.M., 1993. An edge crack torsion method for mode III delamination fracture testing. Journal of Composite Technology and Research 15, 193–201, Fall.

Li, J., O'Brien, T.K., 1996. Simplified data reduction methods for the ECT test for mode III interlaminar fracture toughness. Journal of Composite Technology and Research 18, 96–101.

Marat-Mendes, R.M., Freitas, M.M., 2010. Failure criteria for mixed mode delamination in glass fibre epoxy composites. Composite Structures 92, 2292–2298.

de Morais, A.B., Pereira, A.B., 2008. Mixed mode II + III interlaminar fracture of carbon/epoxy laminates. Composites Science and Technology 68, 2022–2027.

de Morais, A.B., Pereira, A.B., 2009. Mode III interlaminar fracture of carbon/epoxy laminates using a four-point bending plate test. Composites Part A – Applied Science and Manufacturing 40, 1741–1746.

de Morais, A.B., Pereira, A.B., de Moura, M.F.S.F., 2011. Mode III interlaminar fracture of carbon/epoxy laminates using the six-point edge crack torsion (6ECT). Composites Part A: Applied Science and Manufacturing 42, 1793–1799.

de Moura, M.F.S.F., Fernandez, M.V.C., de Morais, A.B., Campilho, R.D.S.G., 2009. Numerical analysis of the edge crack torsion test for mode III interlaminar fracture of composite laminates. Engineering Fracture Mechanics 76, 469–478.

Park, O., Sankar, B.V., 2002. Crack-tip force method for computing energy release rate in delaminated plates. Composite Structures 55, 429–434.

Pereira, A.B., de Morais, A.B., 2009. Mixed-mode I + III interlaminar fracture of carbon/epoxy laminates. Composites Part A: Applied Science and Manufacturing 40, 518–523.

Pereira, A.B., de Morais, A.B., de Moura, M.F.S.F., 2011. Design and analysis of a new six-point edge crack torsion (6ECT) specimen for mode III interlaminar fracture characterisation. Composites Part A: Applied Science and Manufacturing 42, 131–139.

Plain, K.P., Tong, L., 2011. An experimental study on mode I and II fracture toughness of laminates stitched with a one-sided stitching technique. Composites Part A: Applied Science and Manufacturing 42, 203–210.

Reddy, J.N., 2004. Mechanics of Laminated Composite Plates and Shells – Theory and Analysis. CRC Press, Boca Raton, London, New York, Washington D.C.

Reeder, J.R., Crews Jr., J.R., 1990. Mixed-mode bending method for delamination testing. AIAA Journal 28, 1270–1276.

Rice, J.R., 1968. A path independent integral and the approximate analysis of strain concentration by notches and cracks. Journal of Applied Mechanics 35, 379–386.

Rigby, R.H., Aliabadi, M.H., 1998. Decomposition of the mixed-mode *J*-integral – revisited. International Journal of Solids and Structures 35, 2073–2099.

Russel, A.J., Street, K.N. 1982. Factors affecting the interlaminar fracture energy of graphite/epoxy laminates. In: Hayashi, T., Kawata, K., Umekawa, S. (Eds.), Progress in Science and Engineering of Composites, ICCM-IV. ASM International, Tokyo, Japan. pp. 279–286.

Sankar, B.V., Sonik, V., 1995. Pointwise energy release rate in delaminated plates. AIAA Journal 33, 1312–1318.

Shivakumar, K.N., Raju, I.S., 1992. An equivalent domain integral method for three-dimensional mixed-mode fracture problems. Engineering Fracture Mechanics 42, 935–959.

da Silva, L.F.M., Estevez, V.H.C., Chavez, F.J.P., 2011. Fracture toughness of a structural adhesive under mixed mode loadings. Materialwissenschaft und Werkstofftechnik 42, 460–470.

Suemasu, H., Kondo, A., Gozu, K., Aoki, Y., 2010. Novel test method for mixed mode II and III interlaminar fracture toughness. Advanced Composite Materials 19, 349–361.

Suhir, E., 1986. Stresses in bi-metal thermostats. Journal of Applied Mechanics 53, 657–660.

Suo, Z., Hutchinson, J.W., 1990. Interface crack between two elastic layers. International Journal of Fracture 43, 1–18.

Szekrényes, A., 2007. Delamination fracture analysis in the G_{II}-G_{III} plane using prestressed composite beams. International Journal of Solids and Structures 44, 3359–3378.

Szekrényes, A., 2009a. Improved analysis of the modified split-cantilever beam for mode III fracture. International Journal of Mechanical Sciences 51, 682–693.

Szekrényes, A., 2009b. Interlaminar fracture analysis in the G_{I}-G_{III} plane using prestressed composite beams. Composites Part A – Applied Science and Manufacturing 40, 1621–1631.

Szekrényes, A., 2011. Interlaminar fracture analysis in the G_{I}–G_{II}–G_{III} space using prestressed composite beams. Journal of Reinforced Plastics and Composites 30, 1655–1669.

Tsai, S.W., 1992. Theory of composite design. Think Composites, Dayton, Paris, Tokyo.

Valvo, P.S., 2012. A revised virtual crack closure technique for physically consistent fracture mode partitioning. International Journal of Fracture 173, 1–20.

Wang, J., Qiao, P., 2004. Novel beam analysis of end notched flexure specimen for mode-II fracture. Engineering Fracture Mechanics 71, 219–231.

Wang, S., Harvey, C.M., 2012. Mixed mode partition theories for one dimensional fracture. Engineering Fracture Mechanics 79, 329–352.

Wilkins, D.J., Eisenmann, J.R., Camin, R.A., Margolis, W.S., Benson, R.A., 1982. Characterizing delamination growth in graphite-epoxy. ASTM Spec. Technol. Publ. 775, 183.

Williams, J.G., 1988. On the calculation of energy release rates for cracked laminates. International Journal of Fracture 36, 101–119.